The structure of small Ta clusters

2005 J. Phys.: Condens. Matter 17 6111

(http://iopscience.iop.org/0953-8984/17/39/001)

INSTITUTE OF PHYSICS PUBLISHING JOURNAL OF PHYSICS: CONDENSED MATTER

J. Phys.: Condens. Matter **17** (2005) 6111–6121 doi:10.1088/0953-8984/17/39/001

The structure of small Ta clusters

Aiqin Jiang[1], **Trevor A Tyson**[1] **and Lisa Axe**[2]

[1] Department of Physics, New Jersey Institute of Technology, Newark, NJ 07102, USA
[2] Department of Civil and Environmental Engineering, New Jersey Institute of Technology, Newark, NJ 07102, USA

Received 4 May 2005, in final form 7 June 2005
Published 16 September 2005
Online at stacks.iop.org/JPhysCM/17/6111

Abstract

The structure of small tantalum clusters is investigated by using molecular dynamics simulations. A structural evolution from polytetrahedral structures to layered Frank–Kasper-type structures is revealed as cluster size increases to $N \sim 100$ atoms. The lowest-energy structures have been located for clusters with $N \leqslant 78$. The bulk-like (bcc) structure becomes the most stable structure beyond $N \sim 100$. The stabilized structure strongly depends on the cooling rate. A structure similar to β-Ta, a σ-type Frank–Kasper structure, can be obtained by rapid cooling. The structural properties of small Ta clusters presented in the paper provide insight into the formation and origin of β-phase Ta. The growth of β-Ta films in practice may be due to the nucleation of Ta clusters with layered Frank–Kasper-type structure during the initial stage of film growth.

1. Introduction

Nanometre-size particles, or clusters, are of considerable interest due to their fundamental and practical importance. In addition to the increased utilization in catalysis (especially for metallic clusters) and possible technological applications in optoelectronic devices, clusters provide unique systems to understand how the electronic and structural properties of nanoparticles are affected by their size, and in particular how the behaviour of the bulk materials is approached. The structure of a cluster is a key determinant in many of its properties. The delicate balance between surface and internal energies often produces a complex dependence of structure upon cluster size [1, 2]. Atomic clusters of metals are not simply fragments of bulk materials, they can occur in stable arrangements quite different from the bulk crystal structure. With increasing size, the bulk structure begins to dominate. Some clusters of fcc metals, such as aluminium [3, 4], gold [5–7] and lead [8–10], have been extensively studied. Monatomic metal clusters have been observed to exhibit interesting polytetrahedral structures [4, 11–14].

Our study on tantalum clusters was motivated by the need to understand the stability and origin of metastable β-Ta in deposited thin films. Ta films are very useful in the microelectronics industry, especially as an underlayer material in computer integrated circuits [15, 16]. Bcc (α-phase, the bulk structure of tantalum) and the metastable tetragonal

β-phase are the two crystalline phases exhibited in Ta thin films. The structure of deposited thin films is usually the metastable β-phase or a mixture of two phases. Special attention has been paid to the mechanisms of stabilizing the β-phase.

In our previous work [17], molecular dynamics (MD) simulations were performed on tantalum clusters to investigate the stability of the β-Ta phase. It was predicted that the bcc structure is the most stable phase for tantalum clusters with $N > \sim 200$. In this paper, we mainly focus on tantalum clusters with $N < 200$, to study the effect of size on structure and find configurations of greatest stability. The structure optimization is performed by MD simulated annealing. Somewhat surprising results are revealed about the structural evolution of Ta clusters with size. The region at which bcc, the preferred bulk structure, is the most stable structure is also determined. The effects of cooling rate on the stabilized structure of clusters are evaluated. The results presented in this paper provide insights into the formation and origin of β-Ta phase in thin films.

2. Computational detail

2.1. Ta potential

The tantalum clusters were modelled using an embedded-atom-method (EAM) potential and the force-matching method [18, 19], given by

$$E_{\text{tot}} = \sum_i F_i(\rho_i) + \tfrac{1}{2} \sum_{\substack{i,j \\ i \neq j}} V_{ij}(r_{ij})$$

$$\rho_i = \sum_j \phi(r_{ij}).$$

Here E_{tot} is the total energy, $F_i(\rho_i)$ is the embedding energy function, $V_{ij}(r_{ij})$ is the pair potential resulting from electrostatic interactions, and r_{ij} is the distance between atoms i and j. $\phi(r_{ij})$ is the spherically averaged atomic electron density contribution from atom j to atom i. These three functions for Ta have been fitted to a variety of experimental data, equation of state data, and first-principles data including hundreds of DFT forces from a variety of structures such as clusters, surfaces, interstitials, vacancies, liquids, and stacking faults as well as bulk crystal structures at different temperatures [19]. The potential can be applied to calculating equilibrium as well as nonequilibrium properties for Ta. Compared with other empirical potentials previously proposed [20–23], the EAM potential is a preferred approach for describing the properties of Ta clusters and the β-Ta phase. In the EAM potential, the effective interactions between atoms are environment dependent; it is capable of the describing metal surfaces adequately. This approach has been successfully employed to calculate, for example, the energy of relaxation of unreconstructed surfaces (e.g. low-index surfaces of Cu, Ag, Au, Ni, Pd, and Pt) [24–26], surface phonons ((111) surfaces of Cu and Ag) [27], and adatom clusters on Pt(100) [28].

The three functions $V(r)$, $\phi(r)$ and $F(\rho)$ together determine the cluster structure [19]. $F(\rho)$ has a rather broad range of minima around $\rho = 1.0$ [19], and energy loss is not so severely associated with ρ values that deviate from one. Thus surface contraction is not as pronounced as it is for other metallic systems such as lead [29]. Both electron density $\phi(r)$ and pair potential $V(r)$ have a cut-off value of 3.987 Å [19], which normally occurs between the second and third shells. $\phi(r)$ shows much smaller values and slower decay near the cut-off distance than at short distances, and therefore the major contribution around each atom comes from nearest neighbours. $V(r)$ has one minimum value of $-0.463\,17$ eV at $r = 3.0106$ Å [19],

which is located between the first and second shells. The largest contribution to pair potentials comes from the first two shells.

2.2. *Molecular dynamics*

Molecular dynamics was performed using the IMD code originally developed by Stadler [30, 31], and in the canonical ensemble with Nosé–Hoover thermostat [32, 33]. The time step was chosen as 3.5 fs throughout all simulations. Typically runs consist of three steps, first melting a cluster at a temperature above its melting point (approximately 0.35 ns, 1×10^5 time steps); then cooling it down to a temperature under which the cluster is solidified (1×10^7 time steps); and finally continuing the cooling process to 0 K with a greater cooling rate (1×10^6 time steps), as in this case the cluster structure is not expected to be influenced considerably by the rate once it solidifies. However, the re-solidified structures of clusters heavily depend on the cooling rate in the second step, which sometimes needs to take two to ten times longer for large clusters to obtain the equilibrium configurations. The end structures are obtained from the average over 100 time steps after the cluster was brought to thermal equilibrium at 0 K, which was further reoptimized using the basin-hopping [34, 35] (or Monte Carlo minimization [36]) approach with tolerances of 10^{-5} for the root-mean-square force.

The structure optimization calculations are based on the simulated annealing methods [37, 38]. First a cluster is melted to the liquid state, which has a random configuration without any *a priori* assumptions about the optimal structure. By decreasing temperature slowly to 0 K, there is a good chance that the system will settle into the global minimum. While the simulation does not guarantee that the true global minimum will be reached, it often brings the system into a good proximity. Tests on several aluminium clusters of 23, 26, 29, and 55 atoms produced the same structures as the global minima located by Doye [4] with the basin-hopping approach [34, 35]. From our experience, good results can be obtained for small size metallic clusters by MD simulations using EAM potentials. The re-optimization with basin-hopping did not significantly improve the optimized structures obtained from MD simulations, while the tighter convergence criteria can provide more precise coordinates of atoms and total energies of clusters. An empirical potential is used for computational efficiency; *ab initio* electronic structure methods are prohibitively expensive for cluster sizes considered here, especially for a heavy element like tantalum. Therefore, tests on small Ta clusters of seven and 13 atoms were performed using Gausssian03 (LDA) with the LanL2DZ basis sets [39]. The optimized structures have the same point groups as obtained by MD simulations; however, the atomic distances for the first nearest neighbours are on average 5.59% (Ta_7, in a range of 0.18–11.64%) and 4.12% (Ta_{13}, 1.56–6.51%) smaller than MD methods. Similar tests on Al clusters produced again the same point groups as the global minima found by Doye [4], and with atomic distances for nearest neighbours reduced by 8.08% (Al_7, with a range of 0.27–30.62%) and 3.50% (Al_{13}, 0.11–9.96%).

3. Results and discussion

3.1. *Structure of tantalum clusters with size* $N \leqslant 78$

The total energies and average atom potentials of the best minima obtained for the Ta clusters with sizes from 4 to 78 are shown in table 1, for comparison with any future and similar work on Ta clusters. The total energies of clusters were fitted to the following expansion in N [40, 41]:

$$E = aN + bN^{2/3} + cN^{1/3} + d$$

yielding $a = -8.3511$, $b = 6.6273$, $c = -8.5636$, and $d = 8.3643$. The difference between

Table 1. A summary of total energies and average atom energies of the best minima found for a Ta cluster with $N = 4$–78.

Cluster size N	Total energy (eV)	Energy/atom (eV)	Cluster size N	Total energy (eV)	Energy/atom (eV)
4	−22.122 776 26	−5.530 694 07	42	−291.861 862 8	−6.949 091 97
5	−28.543 280 66	−5.708 656 13	43	−299.029 106 5	−6.954 165 27
6	−35.187 154 08	−5.864 525 68	44	−306.581 591 6	−6.967 763 45
7	−41.891 407 20	−5.984 486 74	45	−313.656 434 3	−6.970 142 98
8	−48.345 976 34	−6.043 247 04	46	−321.299 306 9	−6.984 767 54
9	−55.195 737 73	−6.132 859 75	47	−328.575 492 0	−6.990 967 92
10	−62.119 716 48	−6.211 971 65	48	−336.082 004 9	−7.001 708 44
11	−68.966 993 64	−6.269 726 70	49	−343.047 379 5	−7.000 966 93
12	−76.174 669 70	−6.347 889 14	50	−350.241 476 4	−7.004 829 53
13	−84.167 877 82	−6.474 452 14	51	−357.759 539 6	−7.014 892 93
14	−90.487 125 34	−6.463 366 10	52	−365.014 581 6	−7.019 511 19
15	−97.818 551 20	−6.521 236 75	53	−372.139 615 2	−7.021 502 17
16	−104.542 871 5	−6.533 929 47	54	−379.587 929 7	−7.029 406 11
17	−111.173 599 9	−6.539 623 52	55	−387.161 825 9	−7.039 305 93
18	−118.305 426 1	−6.572 523 67	56	−394.723 902 0	−7.048 641 11
19	−126.109 469 7	−6.637 340 51	57	−402.342 840 1	−7.058 646 32
20	−132.894 284 1	−6.644 714 21	58	−409.750 322 3	−7.064 660 73
21	−140.024 874 3	−6.667 851 16	59	−417.279 865 2	−7.072 540 09
22	−147.419 125 9	−6.700 869 36	60	−424.657 049 1	−7.077 617 49
23	−154.435 984 9	−6.714 608 04	61	−432.134 384 6	−7.084 170 24
24	−161.269 754 3	−6.719 573 10	62	−439.236 891 5	−7.084 465 99
25	−168.520 065 7	−6.740 802 63	63	−446.770 533 6	−7.091 595 77
26	−175.893 699 1	−6.765 142 27	64	−454.216 379 4	−7.097 130 93
27	−182.725 405 7	−6.767 607 62	65	−461.353 938 0	−7.097 752 89
28	−190.091 736 4	−6.788 990 59	66	−468.758 888 0	−7.102 407 39
29	−197.598 194 6	−6.813 730 85	67	−476.130 491 3	−7.106 425 24
30	−204.488 600 1	−6.816 286 67	68	−483.438 444 4	−7.109 388 89
31	−211.558 410 9	−6.824 464 87	69	−491.032 223 7	−7.116 409 04
32	−219.260 481 5	−6.851 890 05	70	−498.243 681 0	−7.117 766 87
33	−226.201 685 4	−6.854 596 53	71	−505.862 863 9	−7.124 829 07
34	−233.499 115 0	−6.867 621 03	72	−513.287 634 8	−7.128 994 93
35	−240.846 400 9	−6.881 325 74	73	−520.710 743 7	−7.133 023 89
36	−248.024 788 8	−6.889 577 47	74	−528.100 972 9	−7.136 499 63
37	−255.318 422 4	−6.900 497 90	75	−535.966 901 0	−7.146 225 35
38	−262.447 955 1	−6.906 525 13	76	−543.842 686 9	−7.155 824 83
39	−270.120 312 5	−6.926 161 86	77	−551.518 206 7	−7.162 574 11
40	−277.241 578 0	−6.931 039 45	78	−559.162 089 6	−7.168 744 74
41	−284.376 284 3	−6.936 006 94			

the calculated minimum and best fit presented in figure 1 highlights the stable clusters [4, 42]. A selection of stable clusters with interesting structure features is depicted in figure 2. Simulations predicted these particularly stable clusters with sizes $N = 13$, 15, 19, 22 and 29, which are consistent with the magic numbers reported for Ta obtained from time-of-flight (TOF) mass spectra [43]. Most structures with 4–14 atoms are on a polytetrahedral growth sequence, except for the six-atom octahedron and the eight-atom dodecahedron. The seven-atom cluster has a pentagonal bipyramid shape and the 13-atom cluster is icosahedra. 15-atom and 16-atom clusters show Z14 and slightly off-centred Z15 coordination polyhedra, respectively, which was defined by Frank and Kasper [44, 45] for complex alloy structures. Metastable β-Ta was

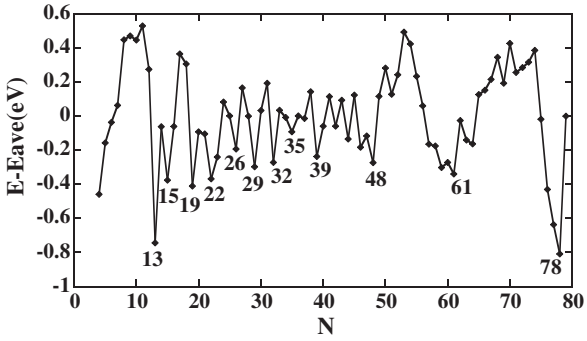

Figure 1. Energies of best minima relative to E_{ave}, a four-parameter fit to their energies. $E_{\mathrm{ave}} = -8.3511N + 6.6273N^{2/3} - 8.5636N^{1/3} + 8.3643$.

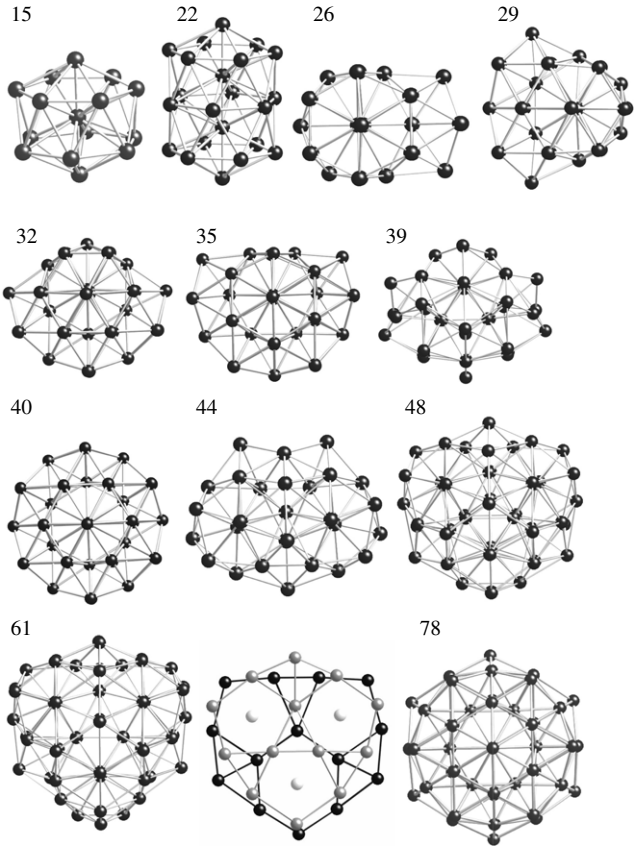

Figure 2. A selection of clusters with particular stable structure. Each cluster is labelled by the value of N.

determined to belong to σ-type Frank–Kasper structure with a self-hosting feature [46, 47]. The 19-atom Ta cluster is a double icosahedron. Starting from 22 atoms, growth occurs around the double Z14 polyhedron with atoms being added above the faces and vertices of this structure.

Subsequently, a series of interpenetrating 13-atom icosahedra forms with their centres located on a hexagon, which is a part of 22-atom double Z14 polyhedron. The growth leads to the stable structures with $N = 26$, 29, 32 and 35 (figure 2). In contrast to aluminium clusters, beyond $N = 13$, growth occurs by adding atoms around 13-atom icosahedra [4], rather than a 22-atom double Z14 polyhedron, indicating that tantalum clusters have a higher tendency to form sixfold rather than fivefold symmetric structures as compared to Al clusters. The 40-atom Ta cluster has a perfect ring of six interpenetrating icosahedra around the double Z14 polyhedron centre, which is same as the global minimum of the 40-atom aluminium cluster. Similar structures have previously been found for Dzugutov clusters [48, 49]. The 40-atom cluster forms an oblate spheroid with a large surface area, which reduces its stability. However, the 39-atom cluster rearranges to form a more stable structure with a high symmetry distinct from the 40-atom cluster.

The interpenetrating Z14 and Z15 polyhedra lead to stable clusters at $N = 44$, 48, and 61 atoms. These are based on the Frank–Kasper-type phase, planar layering of atoms. The primary layers (those in which atoms are in contact) are tessellations of hexagons, pentagons and triangles. An interlayer of atoms centres the superposed hexagons or pentagons to complete a well coordinated structure (see the layers cut from the 61-atom cluster in figure 2). The stable 78-atom cluster has the same symmetry as the 40-atom cluster but with a near doubling of size, because it has four interpenetrating Z14 polyhedra at the centre with atoms around them forming a nearly spherical surface. This cluster can be seen as a small fragment cut from σ-type Frank–Kasper structure to which β-Ta belongs (figure 2).

The observed structures are a consequence of many-body interatomic interactions. The Ta potential functions determine the tendency of small Ta clusters to form Z14 polyhedra with over-stacked hexagons. The embedding function directly depends on the averaged electron density, hence it is relatively insensitive to the pair distances and coordination numbers. The high coordination numbers in Z14 and Z15 polyhedra can help achieve an electron density near $\sim$1 [19] (the embedding function $F(\rho)$ has a rather broad range of minima around $\rho = 1.0$, discussed in section 2.1), but with a wide distribution of nearest-neighbour distances resulting in internal strains in the disordered clusters [4, 50].

3.2. Structural transition near $N \sim 100$

As the cluster size increases, the probability of locating the global minimum decreases because the number of minima increases exponentially with N [51–53]. Simulated annealing was performed on clusters of $\sim$100 atoms, including 88-, 95-, 102-, 119- and 147-atom clusters, which resulted in layered Frank–Kasper-like structures. The energies of end structures strongly depend on the cooling rate. Slow cooling often improves the minima; nevertheless, attaining the global minima is difficult. Several runs were conducted with different cooling rates (2×10^7, 4×10^7 and 1×10^8 steps, cooling from 1798 to 696 K) on the cluster with 175 atoms, which is a magic number of a rhombic dodecahedron cluster cut from the bcc lattice. The stabilized structures resulted in the σ-like Frank–Kasper structure, with slight surface modification. However, they have much higher energies than that of the relaxed bcc 175-atom cluster, so clearly the Frank–Kasper type structure is not the most stable structure. Interestingly, we found that the 169-atom tantalum liquid can be stabilized to a bcc structure, a truncated rhombic dodecahedron, which is formed by removing six atoms at vertices on (100) bcc lattice planes from a 175-atom bcc polyhedron. The 169-atom cluster is the smallest one for which we observed the bcc formation from liquid in MD simulations. The 369-, 671- and 1105-atom clusters were also observed to stabilize into the bcc structure. Therefore, the transition to bulk bcc most likely occurs with sizes less than 169 atoms.

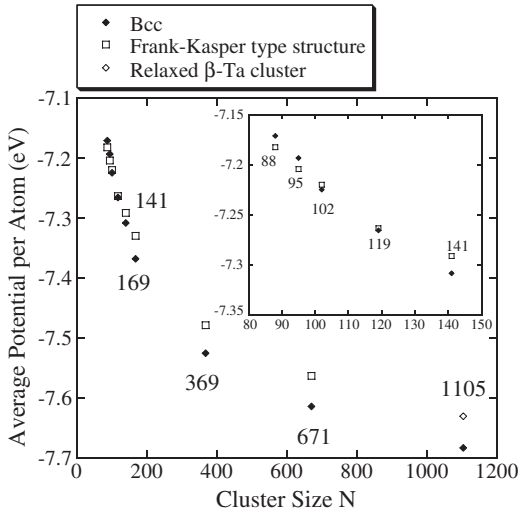

Figure 3. Plot of averaged potential per atom versus cluster size for bcc and the layered structures (similar to Frank–Kasper phases). The crossover region is expanded.

Table 2. The stabilized structures of large clusters showing strong dependence on cooling rate.

Clusters size N	169			369			671			1105		
Temperature change[a] (K)	1798 → 696			1937 → 1160			2552 → 1392			2669 → 1059		
Time steps	6×10^7	8×10^7	1×10^8	4×10^7	6×10^7	1×10^8	4×10^6	6×10^6	8×10^6	5×10^5	2×10^6	4×10^6
Stabilized structure	F–K[b]	Bcc	Bcc	F–K	Bcc	Bcc	F–K	Bcc	Bcc	Bcc	Bcc	Bcc

[a] Temperature change is for the second step of simulations (see section 2.2), which was followed by the third step, continuing cooling to 0 K with a greater cooling rate.
[b] F–K represents the σ-type Frank–Kasper structure, which β-Ta belongs to.

Bcc clusters were constructed with 88, 95, 102, 119 and 141 atoms by truncating the optimized 169-atom bcc cluster. Simulated annealing with different cooling rates always stabilizes each of them into similar layered structures. To assess whether the bcc structure exhibits a lower energy than the layered structure, ten internal atoms of these initial bcc clusters were fixed during the entire simulation (melting and cooling) to force the formation of bcc. The averaged potentials per atom in the final bcc structures are compared with the lowest potentials we obtained for layered structures in figure 3; a crossover is seen near $N \sim 100$ (see the enlarged crossover part inserted in figure 3). The bcc (88-, 95-atom) clusters have higher energies than their corresponding Frank–Kasper-type structures, indicating bcc is not stable for clusters of $N \lesssim 100$. The potential difference for sizes between ∼100 and 120 is much less than for clusters with lower (e.g. 88-, 95-atom) or larger (144-, 169-atom) sizes, signifying the structure transition occurs in this region. Above this region, the differences increase with size. The layered Frank–Kasper type structures can be formed for 369, and 671-atom clusters under proper cooling rates, with much higher averaged potentials than the bcc structure (figure 3).

The stabilized configuration strongly depends on the cooling rate. There is a high tendency of forming the Frank–Kasper type structure with rapid cooling, which has fewer time steps for a given temperature change (table 2). However, with smaller clusters, a slower cooling rate is

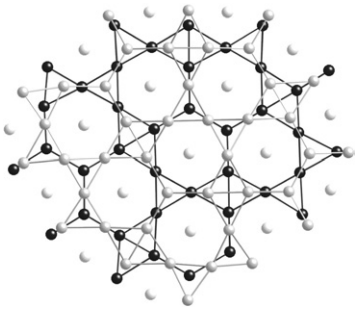

Figure 4. The atomic layers in 369-atom cluster having β-phase structure.

sometimes required for the stabilizing β-Ta type structure (table 2) because of the impact of a relatively higher surface energy. As the cluster gets big enough, bcc can be easily obtained even with a rapid cooling. For example, bcc was formed for the 1105-atom cluster, using 5×10^5 steps and cooling from 2669 to1059 K. A melted 1105-atom cluster was not observed to form the β-Ta type structure with selected cooling rates (table 2) in our simulations. In order to sketch the trend of potentials for the Frank–Kasper structures of large clusters, a ball β-Ta cluster cut from the β-phase lattice with 1105 atoms was constructed. The cluster was first relaxed at temperature near their melting points (but not melted) and then cooled slowly to 0 K. Because no phase change occurs for the pure β-Ta clusters [54], the end cluster still exhibits a Frank–Kasper-type structure. Its averaged potential was incorporated in figure 3, providing a convincing prediction of potential trends for the two types of structures as size increases. Therefore, we conclude that the bcc structures become lowest in energy beyond $N \sim 100$.

3.3. Formation of β-phase Ta

MD simulations revealed that as size increases tantalum clusters start with polytetrahedral structures, and gradually evolve into layered structures, which are based in some way on Frank–Kasper phases. For clusters of $N > 100$ atoms, the bcc structure becomes the lowest-energy structure. However, the melted clusters in the range of ∼100–200 atoms hardly form bcc structures in our simulations; and the stabilized structure strongly depends on the cooling rate for small clusters. Rapid cooling can result in the formation of the β-phase. However, as the cluster size increases the bcc configuration dominates.

The 369- and 671-atom clusters can form either a bcc structure or the Frank–Kasper-type phase, depending on the cooling rate. The stabilized 369-atom cluster with Frank–Kasper-type structure has almost the same atomic layer arrangement as the β-Ta (figure 4), with a slight surface distortion. This structure has primary hexagonal–triangular, Kagome-tiling nets with three kinds of vertices (3636, $3^2 6^2$, 6^3) (figure 4). The pseudohexagons in the nearest two primary nets are antisymmetrically superposed. An interlayer of a square-triangle net $3^2 434$ centres the superposed hexagons between primary layers, forming series of interpenetrating Z14 polyhedra. The radial distribution functions of 369- and 671-atom clusters with β-Ta type structure were compared to that of a relaxed 5005-atom β-Ta cluster at 0 K in figure 5. They have almost the same distance range of ∼2.6–3.0 Å for nearest neighbours. Compared to the 5005-atom cluster, the broadened peaks and low amplitude (especially at long distances) for 369- and 671-atom clusters are due to the relatively large percentage of atoms on the surface.

The structural evolution of Ta clusters of fewer than ∼100 atoms and formation of β-phase for large clusters ($N > \sim 100$) provide insights into the β-phase formation in depositing Ta

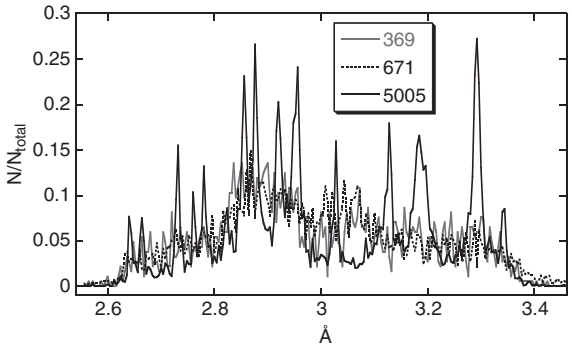

Figure 5. The radial distribution functions of 369- and 671-atom clusters with σ-type Frank–Kasper structure, in comparison with that of a relaxed 5005-atom β-Ta cluster at 0 K.

thin film. Substrate temperature was found to be one of the most important factors in controlling the crystal structure of the deposited Ta film [55–58]. The high substrate temperatures promote the formation of bcc Ta over the β-phase. Sputtering on substrates which are not preheated or are heated solely by the sputtering process yields a tetragonal β-phase. This can be attributed to the limited mobility of Ta atoms in the growing films at low temperatures. Similarly in our MD simulations, the rapid cooling does not provide atoms with enough time to rearrange themselves and locate the lowest-energy positions. Substrate temperatures reported to produce a completely bcc phase coating using an argon sputtering gas have typically been greater than 300 °C and as high as 600 °C [57–60].

Interesting structures of small Ta clusters may be associated with nucleation of Ta atoms during the deposition process. If Ta atoms are sputtered in clusters and not an atomic process, a hypothesis proposed by Collobert and Chouan [59], the structure of the resulting films depends critically on the properties of the deposited clusters. Once the particular stable structure of the created cluster is nucleated, the growth of grains can maintain that particular structure. For example, β-phase grains would be expected to form if Z14 polyhedron clusters with sizes of 15, 22, 26, 29 are created and nucleated.

Of course, the structures of the created clusters strongly depend on the deposition conditions. Recently Arakcheeva and Chapuis [60] reported their experimental work on Ta clusters with Frank–Kasper σ-type structure. The temperature-dependent evolution of the clusters leads to two phase transformations at 65 and 150 K which are related to the electrical and magnetic properties. It was suggested that the nature of the stabilization of β-Ta at the cathode is due to the high electron density on the cathode surface, and its Frank–Kasper σ-type structure can only be stabilized as negatively charged crystallization nuclei [61]. Klaver and Thijsse [61] found that a heavily distorted bcc cluster with 22 atoms was created by bombarding a β-Ta film with argon ions in a simulated deposition system [61]. Substrate properties are important in controlling the phase of Ta films. Heteroepitaxy phenomena have been reported frequently in the phase formation of Ta films [62–68]. Some substrates, such as a bcc-Nb sublayer [62–65], titanium [66, 67] and (111)-oriented Al layers [68], preferentially produce α-Ta. The epitaxial effect could make it difficult to nucleate polytetrahedral structures as seen for the free-standing clusters in our MD study. Lastly, there has been some discussion about whether β-Ta is an impurity-stabilized phase [69–72]. Our investigation on the free-standing clusters clearly shows that the β-phase can be developed without impurities. The β-phase exists as an intrinsic phase at low cluster sizes.

4. Conclusion

In this paper, we have presented an MD study on small size tantalum clusters described by an EAM potential. As cluster size increases, the structure evolves from polytetrahedra into the layered Frank–Kasper-like structure up to $N \sim 100$. The structural transition to bcc, the bulk-like structure, occurs near $\sim$100, beyond which bcc is the lowest-energy structure. The stabilized structure strongly depends on the cooling rate in the simulation, as with rapid cooling the β-Ta structure, a σ-type Frank–Kasper structure, formed for large clusters.

The properties of these clusters can provide useful insights into the origin of β-phase Ta and its mechanism of formation. The structures of stabilized small tantalum clusters play an important role in the phase formation of thin films. Nucleation of clusters with layered Frank–Kasper type structures may preferentially promote the growth of β-Ta film. The theoretical prediction of β-phase for the free-standing pure Ta clusters confirms that the metastable structure is an intrinsic phase of Ta evolving from small-size clusters.

References

[1] Raoult B, Farges J, De Feraudy M F and Torchet G 1989 *Phil. Mag.* B **60** 881
[2] Cleveland C L, Landman U, Schaaff T G, Shafigulllin M N, Stephens P W and Whetten R L 1997 *Phys. Rev. Lett.* **19** 1873
[3] Turner G W, Johnson R L and Wilson N T 2000 *J. Chem. Phys.* **112** 4773
[4] Doye J P K 2003 *J. Chem. Phys.* **119** 1136
[5] Ercolessi F, Andreoni W and Tosatti E 1991 *Phys. Rev. Lett.* **66** 911
[6] Lewis L J, Jensen P and Barrat J-L 1997 *Phys. Rev.* B **56** 2248
[7] Michaelian K, Rendo'n N and Garzo'n I L 1999 *Phys. Rev.* B **60** 2000
[8] Hendy S C and Hall B D 2001 *Phys. Rev.* B **64** 085425
[9] Hendy S C and Doye J P K 2002 *Phys. Rev.* B **66** 235402
[10] Doye J P K and Hendy S C 2003 *Eur. Phys. J.* D **22** 99
[11] Wang G M, Blaisten-Barojas E, Roitberg A E and Martin T P 2001 *J. Chem. Phys.* **115** 3640
[12] Dassenoy F, Casanove M-J, Lecante P, Verelst M, Snoeck E, Mosset A, Ould Ely T, Amiens C and Chaudret B 2000 *J. Chem. Phys.* **112** 8137
[13] Nelson D R and Spaepen F 1989 *Solid State Phys.* **42** 1
[14] Doye J P K and Wales D J 2001 *Phys. Rev. Lett.* **86** 5719
[15] Holland L (ed) 1965 *Thin Film Microelectronics* (New York: Wiley)
[16] Maissel L I and Francombe M H 1973 *An Introduction to Thin Films* (New York: Gordon and Breach)
[17] Jiang A, Tyson T A, Axe L, Gladczuk L, Sosnowski M and Cote P 2005 *Thin Solid Films* **479** 166–73
Jiang A, Tyson T A and Axe L 2005 *J. Phys.: Condens. Matter* **17** 1841–50
[18] Daw M S and Baskes M I 1984 *Phys. Rev.* B **29** 6443
[19] Li Y, Siegel D J, Adams J B and Liu X-Y 2003 *Phys. Rev.* B **67** 125101
[20] Guellil A M and Adams J B 1992 *J. Mater. Res.* **7** 639
[21] Finnis M W and Sinclair J E 1984 *Phil. Mag.* A **50** 45
[22] Wang G, Strachan A, Cagin T and Goddard W A III 2001 *Mater. Sci. Eng.* A **309/310** 13
[23] Lee B-J, Baskes M I, Kim H and Cho Y K 2001 *Phys. Rev.* B **64** 184102
[24] Daw M S and Baskes M I 1983 *Phys. Rev. Lett.* **50** 1285
Daw M S and Baskes M I 1984 *Phys. Rev.* B **29** 6443
Foiles S M, Baskes M I and Daw M S 1986 *Phys. Rev.* B **33** 7983
Foiles S M, Baskes M I and Daw M S 1988 *Phys. Rev.* B **37** 10387
Daw M S 1989 *Phys. Rev.* B **39** 7441
[25] Ercolessi F, Parrinello M and Tosatti E 1988 *Phil. Mag.* A **58** 213
[26] Chen S P, Voter A and Srolovitz D L 1980 *Phys. Rev.* B **22** 1564
Voter A F and Chen S P 1987 *Mater. Res. Soc. Symp. Proc.* **82** 175
[27] Nelson J S, Daw M S and Sowa E C 1989 *Phys. Rev.* B **40** 1465
[28] Schwoebel P, Foiles S M and Kellogg G 1989 *Phys. Rev.* B **40** 10639
Wright A F, Daw M S and Fong C Y 1990 *Phys. Rev.* B **42** 9409
Chen S P, Srolovitz D J and Voter A F 1989 *J. Mater. Res.* **4** 62

[29] Lim H D, Ong C K and Ercolessi F 1992 *Surf. Sci.* **269/270** 1109
[30] Stadler J, Mikulla R and Trebin H-R 1997 *Int. J. Mod. Phys.* C **8** 1131
[31] Roth J, Gähler F and Trebin H-R 2000 *Int. J. Mod. Phys.* C **11** 317
[32] Nosé S 1984 *J. Chem. Phys.* **81** 511
[33] Nosé S 1984 *Mol. Phys.* **52** 255
[34] Wales D J and Scherag H A 1999 *Science* **285** 1368
[35] Wales D J and Doye J P K 1997 *J. Phys. Chem.* A **101** 5111
[36] Li Z and Scheraga H A 1987 *Proc. Natl Acad. Sci. USA* **84** 6611
[37] Metropolis N, Rosenbluth A W, Rosenbluth M N, Teller A H and Teller E 1953 *J. Chem. Phys.* **21** 1087
[38] Kirkpatrick S, Gelatt C D and Vecchi M P 1983 *Science* **220** 671
[39] Frisch E, Frisch M J and Trucks F W 2003 *Gaussian03 User's Reference* (Pittsburg, PA: Gaussian)
[40] Northby J A, Xie J, Freeman D L and Doll J D 1989 *Z. Phys.* D **12** 69
[41] Northby J A, Xie J, Freeman D L and Doll J D 1989 *J. Chem. Phys.* **91** 612
[42] Doye J P K and Hendy S C 2003 *Eur. Phys. J.* D **22** 99
[43] Sahurai M, Watanabe K, Sumiyama K and Suzuki K 1999 *J. Chem. Phys.* **111** 235
[44] Frank F C and Kasper J S 1958 *Acta Crystallogr.* **11** 184
[45] Frank F C and Kasper J S 1959 *Acta Crystallogr.* **11** 483
[46] Arakcheeva A, Chapuis G and Grinevitch V 2002 *Acta Crystallogr.* B **58** 1
[47] Arakcheeva A, Chapuis G, Birkedal H, Pattison P and Grinevitch V 2003 *Acta Crystallogr.* B **59** 324
[48] Doye J P K, Wales D J and Simdyankin S I 2001 *Faraday Discuss.* **118** 159
[49] Doye J P K and Wales D J 2001 *Phys. Rev. Lett.* **86** 5719
[50] Baletto F, Ferrando R, Fortunelli A, Montalenti F and Mottet C 2002 *J. Chem. Phys.* **116** 3856
[51] Tsai C J and Jordan K D 1993 *J. Phys. Chem.* **97** 11227
[52] Stillinger F H 1999 *Phys. Rev.* E **59** 48
[53] Doye J P K and Wales D J 2002 *J. Chem. Phys.* **116** 3777
[54] Jiang A, Tyson T A and Axe L 2005 *J. Phys.: Condens. Matter* **17** 1841
[55] Schauer A and Roschy M 1972 *Thin Solid Films* **12** 313
[56] Fischer D, Meissner O, Schreiber J, Stavrev M and Wenzel C 1997 *Surf. Interface Anal.* **25** 522
[57] Matson D W, McClanahan E D, Rice J P, Lee S L and Windover D 2000 *Surf. Coat. Technol.* **133/134** 411
[58] Charles S and Whitman J 2000 *Vac. Sci. Technol.* B **18** 2842
[59] Collobert D and Chouan Y 1978 *Thin Solid Films* **55** L15
[60] Arakcheeva A and Chapuis G 2005 *Europhys. Lett.* **69** 378
[61] Klaver P and Thijsse B 2002 *Thin Solid Films* **413** 110
[62] Sajovec F, Meuffels P M and Schober T 1992 *Thin Solid Films* **219** 206
[63] Lee S L, Cipollo M, Windover D and Rickard C 1999 *Surf. Coat. Technol.* **120** 44
[64] Lee S L and Windover D 1998 *Surf. Coat. Technol.* **108/109** 65
[65] Matson D W, McClanahan E D, Rice J P, Lee S L and Windover D 2000 *Surf. Coat. Technol.* **133/134** 411
[66] Chen G S, Chen S T, Huang S C and Lee H Y 2001 *Appl. Surf. Sci.* **169/170** 353
[67] Sato S 1982 *Thin Solid Films* **94** 321
[68] Hoogeveen R, Moske M, Geisler H and Samwer K 1996 *Thin Solid Films* **275** 203
[69] Croset M and Velasco G 1972 *J. Vac. Sci. Technol.* **9** 165
[70] Hieber K 1974 *Thin Solid Films* **24** 157
[71] Morsbito J M 1974 *Anal. Chem.* **46** 189
[72] Schwartz N, Reed W A, Polash P and Read M H 1972 *Thin Solid Films* **14** 333